Green Chemistry

PAPER

View Article Online
View Journal | View Issue

Cite this: *Green Chem.*, 2023, **25**, 399

Oxide ceramic electrolytes for all-solid-state lithium batteries – cost-cutting cell design and environmental impact†

Andrea Schreiber,‡[a] Melanie Rosen,‡[b] Katja Waetzig,[c] Kristian Nikolowski,[c] Nikolas Schiffmann,[d] Hartmut Wiggers,[e] Michael Küpers,[b] Dina Fattakhova-Rohlfing,[b,e] Wilhelm Kuckshinrichs,[a] Olivier Guillon[b,f] and Martin Finsterbusch*[b,f]

All-solid-state batteries are a hot research topic due to the prospect of high energy density and higher intrinsic safety, compared to conventional lithium-ion batteries. Of the wide variety of solid-state electrolytes currently researched, oxide ceramic lithium-ion conductors are considered the most difficult to implement in industrial cells. Although their high lithium-ion conductivity combined with a high chemical and thermal stability make them a very attractive class of materials, cost-cutting synthesis and scalable processing into full batteries remain to be demonstrated. Additionally, they are Fluorine-free and can be processed in air but require one or more high temperature treatment steps during processing counteracting their ecological benefits. Thus, a viable cell design and corresponding assessment of its ecological impact is still missing. To close this gap, we define a target cell combining the advantages of the two most promising oxidic electrolytes, lithium lanthanum zirconium oxide (LLZO) and lithium aluminium titanium phosphate (LATP). Even though it has not been demonstrated so far, the individual components are feasible to produce with state-of-the-art industrial manufacturing processes. This model cell then allows us to assess the environmental impact of the ceramic electrolyte synthesis and cell component manufacturing not just on an abstract level (per kg of material) but also with respect to their contributions to the final cell. The in-depth life cycle assessment (LCA) analysis revealed surprising similarities between oxide-based all-solid-state batteries and conventional Li-ion batteries. The overall LCA inventory on the material level is still dominated by the cathode active material, while the fabrication through ceramic manufacturing processes is a major contributor to the energy uptake. A clear path that identifies relevant research and development directions in terms of economic benefits and environmental sustainability could thus be developed to promote the competitiveness of oxide based all-solid-state batteries in the market.

Received 6th September 2022,
Accepted 28th November 2022

DOI: 10.1039/d2gc03368b

rsc.li/greenchem

1. Introduction

Dramatically increasing global energy demand and the simultaneous push toward renewable energy sources are creating a market opportunity for emerging energy storage systems. Conventional lithium ion batteries (LIB) power most handheld devices to date, but their limited energy density,[1] operation temperature, and safety concerns[2] may give new battery technologies unique selling points for commercialization. In particular, all-solid-state batteries (ASBs) are a hot topic, with the major differentiator being the type of solid electrolyte (SE). While the ionic conductivity of most solid electrolytes was initially limited, advances over the past decade have brought them into a competitive position, allowing for application as ion conductive phases in high capacity (mixed cathodes). Additionally, due to their rigid nature, solid electrolytes can

[a]*Systemforschung und Technologische Entwicklung (IEK-STE), Forschungszentrum Jülich GmbH, Wilhelm Johnen Str., 52425 Jülich, Germany*
[b]*Institute of Energy and Climate Research – Materials Synthesis and Processing (IEK-1), Forschungszentrum Jülich GmbH, Wilhelm-Johnen-Str., 52425 Jülich, Germany*
[c]*Fraunhofer Institute for Ceramic Technologies and Systems (IKTS), Winterbergstraße 28, 01277 Dresden, Germany*
[d]*Institute for Applied Materials – Ceramic Materials and Technologies, Karlsruhe Institute of Technology (KIT), Haid-und-Neu-Str. 7, 76131 Karlsruhe, Germany*
[e]*Faculty of Engineering and Center for Nanointegration Duisburg-Essen (CENIDE), Universität Duisburg-Essen, Lotharstraße 1, 47057 Duisburg, Germany*
[f]*Helmholtz Institute Münster (IEK-12), Forschungszentrum Jülich GmbH, Wilhelm-Johnen-Str., 52425 Jülich, Germany. E-mail: m.finsterbusch@fz-juelich.de*
†Electronic supplementary information (ESI) available. See DOI: https://doi.org/10.1039/d2gc03368b
‡Equally contributing authors.

also serve directly as the separator in the cell (*e.g.* in the form of a dense layer of the pure SE). For each role in the cell, the various properties of the SE, like mechanical stability, chemical stability in contact with lithium metal or the cathode active material and ionic and electronic conductivity need to be balanced against each other. To this regard, each of the three major classes of solid electrolytes has its individual advantages and drawbacks, which sometimes can be combined in an advantageous manner.

Polymer solid electrolytes have a low specific density and can form thin and flexible layers, resulting in full cells with high energy density.[3] They can be easily processed using industry relevant processes such as screen-printing or tape-casting, and PEO-based cells are already being commercialized by Bolloré. Nevertheless, they suffer significant drawbacks, such as limited electrochemical stability windows,[4] low thermodynamic stability in contact with metallic lithium,[5] and still very low total ionic conductivities at room temperature.[6] Therefore, the most successful approaches in current research use some amount of liquid additives or ceramic fillers[7] to improve the mechanical and electrochemical properties of the cell. Additionally, while less prone to thermal run-away than conventional liquid electrolytes, polymer electrolytes are still flammable. However, to obtain reasonable conductivities, heating is often required, leading to even smaller operating widows of the thermal management system for polymer based cells, compared to liquid electrolyte based LIBs.

In contrast, sulfide electrolytes have the highest ionic conductivities to date with 25 mS cm^{-1} (ref. 8) and enable full cells with high capacity, exceptional cycling rates, and rate retention.[9] The approach is promising, and some start-ups are working on their first commercialization.[10] However, they also have significant drawbacks. While the ductility of sulfide electrolytes enables cold pressing, eliminating the need for high-temperature sintering steps, it also requires the use of high external pressure during cycling to mitigate contact loss.[11] Due to the limited electrochemical stability window and thermodynamic instability towards lithium metal anodes and oxide cathode active materials, protective coatings have to be implemented in the cell design. Finally, sulfide electrolyte materials tend to form H_2S upon contact with moisture. Both synthesis and processing have to be carried out in dry room or argon atmospheres, making both systematic investigation of the process and upscaling of process routes to an industrially relevant level much more difficult.

The third class of solid electrolytes are the oxide-based materials, which can be further sub-divided into oxides and phosphates.[12] Within the latter, lithium aluminum titanium phosphate (LATP)[13] with its NASICON ((Na)sodium Super Ionic CONductor) structure shows bulk ionic conductivities up to the 5×10^{-3} S cm^{-1} at room temperature,[14] while also exhibiting excellent chemical stability in air and having relatively inexpensive precursor materials. While the instability of LATP in contact with lithium metal[15] prevents its use as a separator material, it can still provide ionic conductivity in the mixed cathode. However, fabrication of thick film cathodes *via* conventional sintering routes is still challenging due to the limited chemical stability of LATP and cathode active materials at elevated temperatures.[16] With the help of newly developed processing technologies such as aerosol deposition, composite LATP-lithium nickel manganese cobalt oxide (NMC) cathodes (also called mixed cathodes) have been successfully demonstrated.[17]

Fully oxide electrolytes such as garnet-type lithium lanthanum zirconium oxide (LLZO) also exhibit sufficient chemical stability in air (after formation of native carbonate surface layer) and excellent electro-chemical stability towards lithium metal,[18] making this material class best suited for the application as solid-state separators. They can also reach competitive ionic conductivities, *e.g. via* Ga-substitution, demonstrating 1.35×10^{-3} S cm^{-1} at room temperature.[19] Their application in mixed cathodes has been successfully demonstrated,[20,21] but their high density is detrimental to the overall energy density of the cell.

LLZO and LATP powders can be prepared by a variety of synthetic methods, ranging from seemingly simple methods such as solid-state synthesis[13,22] or sol–gel[23] to more complex processes such as Pecchini synthesis,[24,25] co-precipitation,[26] flame spray pyrolysis,[27] or glass melting.[28] Nevertheless, the reported stoichiometries of the materials obtained, as well as the physical properties of the battery components produced, vary considerably across reports. However, Mann *et al.*[29] point out that by carefully controlling the stoichiometry and particle size of LLZO *via* different synthesis routes, all the products obtained have the same physical and electrochemical properties. Therefore, for the purpose of this work, we assume that the synthesis method does not affect the quality of the solid electrolyte powder and the properties of the resulting battery components.

Therefore, solid-state synthesis of both LLZO and LATP was used as a baseline technology in this study. This process does not require additives and therefore can be easily chemically balanced, but additional processing steps are required to achieve physical properties such as particle size and morphology suitable for battery manufacturing processes. In addition, two solvent-based synthesis methods, spray-drying of LLZO and sol–gel synthesis of LATP, are considered. These processes are suitable for industry-scale production of these materials.

While the basic material properties can compete with those of other solid-state electrolytes, the major drawback of oxide-based electrolytes is their processing. The need for extensive high temperature treatments during synthesis and component fabrication raises question of environmental and economic competitiveness. Therefore, the objective of this study is to investigate a realistic battery design based on oxide solid-state electrolytes, selected with respect to its economic feasibility and environmental impact, and to point the way for related research and development.

The production processes of LIBs are often energy intensive and require different minerals and metals. Their mining, extraction, and processing also involve high energy consump-

tion and generate emissions and waste. The end-of-life (EoL) processes of LIBs also contribute to environmental impacts.[30–32] Therefore, life cycle analysis (LCA) is needed to quantify the total environmental impact of batteries from a life cycle perspective. Over the past decade, a plethora of articles have been published on the environmental aspects of LIBs, reflecting the high level of interest in this topic from the LCA community. In 2017, Peters *et al.*[33] conducted a literature review on 113 LCA studies of LIBs and battery electric vehicles (BEVs) published between 2000 and 2016. Most of the studies focused on greenhouse gas emissions and energy demand, while other potential impacts (*e.g.*, toxicity, acidification, resource depletion) are less frequently quantified. The authors[33] found only 11 of the 113 studies contained original life cycle inventory (LCI) data and that most of the existing LCA studies were based on LCI data from four well-known studies published in 2010–2014.[34–37] The problem of a weak LCI database has not improved significantly in the last 5 years, with a few exceptions. A recently published study[38] performs a bottom-up analysis of the energy flows of LIB cell production at laboratory scale with new primary in-house electricity measurements at Karlsruhe Institute of Technology (KIT) to fill this data gap and update previously outdated data. In 2018, Peters *et al.*[39] provided a common base for LCA of LIBs by unification of existing LCIs. The GREET (Greenhouse Gases, Regulated Emissions, and Energy Use in Transportation) model (**https://greet.es.anl.gov/**) is a tool that examines the life cycle impacts of vehicles, fuels, and energy systems, including an LCA model for batteries that is continuously updated.[40] Dai *et al.*[41] used the GREET model to analyse the cradle-to-gate total energy use, emissions, and water consumption associated with current industrial production of NMC-based batteries. In addition, this study highlights the differences in LCIs for key battery materials among existing LIB LCA studies. The results show that the environmental impacts of LIBs are dependent on where in the world the battery is produced and where the materials are sourced. The study of Manjong *et al.*[42] also identifies the sources of variabilities (levers) by disaggregating the value chains of six raw battery materials (aluminium, copper, graphite, lithium carbonate, manganese, and nickel). The results convey insights into how changes in the lever settings yield variations in the overall greenhouse gas (GHG) emissions of the raw materials leading towards a more reliable LCA of LIBs.[42] The studies published by Ellingsen *et al.*[43] and Crenna *et al.*[44] compare LCIs of LIBs and identify key assumptions and differences in existing LCA studies to enhance transparency in the underlying assumptions and results obtained. To reduce the previous ranges of 50–500 kg CO_2 eq. per kW per h battery capacity in the various LCA studies on LIBs,[43] the authors[44] provide new modular datasets for LIB chemistry (*e.g.*, using NMC111, NMC811) using the most recent data from existing sources and assessed a wide range of environmental impacts of the modelled chemistries. Chordia *et al.*[45] adopt the original small-scale factory, which was modelled by Ellingsen *et al.*[37] using Ecoinvent v2.2 background datasets, to the latest Ecoinvent v3.7.1 database and use new LCI data to model LIB cell production in a large-scale facility representative of the latest technology in LIB production.

Since the ASBs technology is still in its infancy, there are only a limited in number of published LCAs of ASBs. Lastoskie and Dai[46] compare the environmental impacts of two solid-state battery manufacturing processes: lamination and thin-film vacuum vapour deposition. Various cathode active materials (CAMs) such as lithium cobalt oxide (LCO), lithium manganese oxide (LMO), and lithium vanadium oxide were studied in conjunction with graphite anodes. In 2016, we investigated the production of a mixed cathode of lithium cobalt oxide and LLZO on the laboratory scale to determine the environmental impacts of a pouch ASB cell.[47] Apart from the laboratory production, which represents the current workflow, an idealized laboratory production and a possible industrial production were portrayed as well. The results indicate that electricity consumption plays a major role due to the many high-temperature production steps as already stated for the LIBs.[33,43,44] Keshavarzmohammadian *et al.*[48] studied the environmental impacts of sulphur-based solid-state lithium batteries for use in BEVs. Their results show the highest environmental impacts for different assembly processes. Overall, the operation of the dry room required for Lithium-sulphur battery production is the largest energy consumer and contributes the most to Global Warming Potential (GWP). The work of Rossi *et al.*[49] addressed the question of which battery energy storage systems (BESSs) are most sustainable for solar home systems. For this purpose, they compared several conventional LIBs from previous studies[34,37,50,51] and "theoretical" solid-state LIBs by replacing the liquid electrolyte (*e.g.*, lithium hexafluorophosphate ($LiPF_6$), sodium tetrafluoroborate ($NaBF_4$)) with the same amount of LIPON (Lithium phosphorous oxynitride) in the LCA model. In terms of GWP, Human Toxicity Potential (HTP), and Fossil Depletion (FD), solid-state LIBs with NMC and nickel cobalt aluminium (NCA) CAMs perform best. Smith *et al.*[52] compared the environmental impacts of a LIB with a lithium iron phosphate (LFP) cathode with that of an ASB based on a lithium lanthanum zirconium tantalum oxide (LLZTO) garnet-structured electrolyte. They use two functional units for the LCA, delivery of 50 MJ of electrical energy and 1 kg of battery. For a functional unit of 50 MJ energy delivered, the environmental impact of the LIB is lower across all the environmental impact categories studied. However, relative to a kilogram of battery, the environmental impacts of the LIB are higher in three environmental categories (freshwater and marine ecotoxicity potential ($ET_{Freshwater}$, ET_{Marine}, HTP). To reduce the GWP of the ASB below that of the LIB, ASB would have to reach 2800 cycles. Zhang[53] analyzed the environmental impacts of a typical ASB using LATP. The results are compared with those of conventional LIBs with $LiPF_6$ ethylene carbonate/dimethyl carbonate (EC/DMC). The main drivers of GWP in ASBs are the cathode active material, lithium metal used in the anode, and electricity consumption during certain manufacturing processes. The main drivers of environmental pollution in ASB production are the thickness of LATP electrolyte, the energy-inten-

sive manufacturing processes of LATP (*e.g.*, high stirring and heating energy used to precipitate LATP powder), and the precursors used to prepare oxo-oxalatotitanate ($H_2[TiO(C_2O_4)_2]$). The energy required for full-cell assembly in a glove box was not considered by Zhang[53] although our previous study[47] shows that the energy demand and GWP is considerable (about 30% of the total GWP). The LCA study of Pell and Lindsay[54] quantified the GWP for ASB production in comparison to three commercial LIB chemistries (NMC 811, LFP, lithium-iron-manganese-phosphate). The oxide ASB with NMC 811 shows the lowest GWP with 58 kg CO_2 equivalents per kW per h while the LIB with LPF shows the highest GWP with 78 kg CO_2 equivalents per kW per h. Salado *et al.*[55] provided a general overview of different battery types, followed by an analysis of critical raw materials currently used. They also focused on the more efficient, safer, and environmentally friendly next-generation batteries (ASBs, metal–air batteries, metal-sulfur batteries) and the use of metal–organic frameworks (MOFs) to achieve this. Furthermore, the review addressed battery disposal issues and novel green synthesis methods. Arshad *et al.*[56] identified and reviewed 80 available LCA studies on LIBs, including the studies from Troy[47] as well as Laskostie and Dai[46] mentioned above. For electric batteries, the most analyzed chemistries are LFP, LMO, and NMC, but other chemistries may be used in the future if they continue to evolve. There is also wide variation in the key effect categories (GWP) studied, ranging from 12 to 313 kg CO_2 eq. per kW per h of battery capacity. The authors of this study from 2022[56] again point out that primary data are missing in most of the studies assessed. This emphasizes the importance of a reliable and updated database obtained *via* new LCAs. In highly researched, developing fields of technology such as ASBs outdated databases can lead to erroneous conclusions especially quickly.

2. Deriving a new cell design based on cost-cutting aspects

Figure manufacturing, a mixed-cathode approach and the combination of different solid electrolytes in one cell were chosen to take full advantage of both phosphate- and garnet-based SEs. In addition, we followed the guidelines of the European lithium battery roadmap to define the materials and realistic loadings of the model cell.[57] Guidelines for practical testing and cell design conditions have also been proposed in literature.[58] Due to its high capacity of 180 mA h g^{-1} (ref. 59) and the processability in air, NMC 622 was chosen as the cathode active material. LATP was chosen as the solid electrolyte in the cathode ("catholyte") because of its less expensive raw materials, high compatibility with NMC 622 during processing, and its electrochemical stability up to 4.6 V,[60] which allows full utilization of the capacity of NMC 622.[61] A thickness of 100 μm and a weight ratio of 20 : 80 LATP : NMC are specified for this mixed cathode, corresponding to an areal capacity of 6.15 mA h cm^{-2}. Lithium metal is chosen as the anode active material due to its high energy density. As the amount of lithium ions transferred between the electrodes during reversible cycling is in fact contained in the CAM, we calculated only 10 μm of excess Li metal layer on the anode to compensate for the irreversible Lithium losses during formation cycles. To prevent direct contact of Li metal with LATP, a thin LLZO separator is required to provide a stable and low-impedance interface.[18] The thickness is set at 10 μm, which is at the upper limit for thin film deposition techniques such as physical vapour deposition (PVD) or sol–gel coating, but at the lower limit for tape casting. 10 μm thick Aluminum (Al) and copper (Cu) foils were used as current collectors, again a compromise since the final stacking (bi-polar or parallel) will affect the effective contributions to energy density. This realistic model cell (Fig. 1) has a theoretical energy density of 394.4 W h kg^{-1} but was chosen to represent a feasible cell design that is close to the current state-of-the-art materials and processing technology. It should be explicitly noted that this cell design has not been yet practically implemented. However, the recent breakthrough in processing of various ceramic cell components, such as different mixed ceramic cathodes including tape cast cathode layers,[62] and separators[20] fabricated by different processing techniques,[63,64] pave the way for the realization of the proposed cell in the near future. The chosen cell design leaves room for further improvements, *e.g.*, at the material level (such as coatings and additives) to achieve high capacity utilization and cycling stability, or at the microstructure level, which have already been demonstrated but do not have a major impact on material selection and LCA.[62] For such a cell, the impact of oxide-based solid electrolytes in terms of both the necessary advances in processing technology and

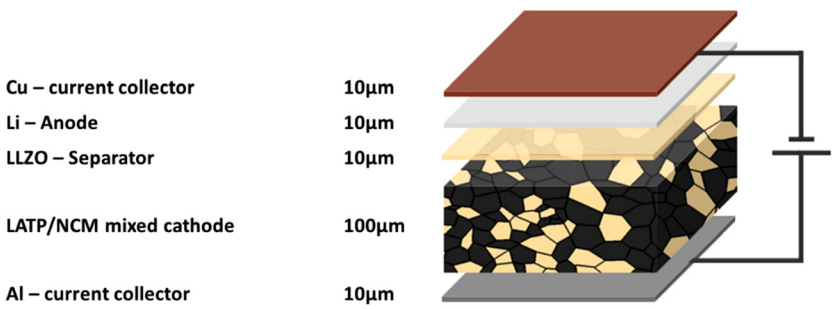

Fig. 1 Model cell set-up for an oxide-based solid-state battery.

their environmental impact at the cell level can now be investigated.

Building on our initial analysis from 2016 [47] and with a significantly improved battery in terms of capacity and energy density, this new LCA is conducted to address the mentioned gaps in the life cycle environmental impacts of ASB cell production. New primary data from laboratory scale studies for material and cell production conducted by the authors were used. Two different synthesis methods for LATP and LLZO powders are analyzed and compared using LCA. A subsequent comparison with the liquid $LiPF_6$ (EC/DMC) electrolyte completes the picture. Within the fixed framework of the model cell (Fig. 1), all deviations in the LCA presented can be contributed to the effects of the specific production route of the cathode and electrolyte and not too different powder and component properties. The LCA results are used to identify the main contributors to the environmental impacts of ASB cell production and to identify strategies to reduce these impacts.

3. Life cycle assessment methodology

LCA is a comprehensive method to assess environmental impacts of products and processes. According to the ISO standards,[65,66] LCA is subdivided into four steps. The goal and scope definition[1] describes the system, the system boundaries, and the functional unit (FU) of the analysis. The LCI[2] compiles and quantifies all material and energy inputs and their subsequent outputs (*e.g.*, emissions, waste, waste heat) on a single process scale along the process chain considered. This includes for example the mining of the necessary materials and energy carriers, their transport and all the production steps required for the investigated system. The life cycle impact assessment (LCIA)[3] evaluates the potential environmental impacts by translating the inputs and outputs gathered in the LCI into environmental effects, so called impact categories. The final interpretation step[4] summarizes the results and draws conclusions to provide recommendations for improvement.

The GaBi 10.6 software[67] is used for modelling the process chains combined with the Ecoinvent 3.7.1 database[68] for background process data (*e.g.* supply of auxiliary material, supply of energy, transport). Most of the primary LCI data of the model cell production (so called foreground data) are provided by the authors. In addition, data already published by us[47] is used in some cases.

The following 18 environmental impacts (Table 1) are calculated using the ReCiPe 2016 v1.1 Midpoint (Hierarchist) methodology[69] implemented in the GaBi software.

3.1 Goal and scope

The objective of the study is to evaluate the environmental impacts associated with the fabrications of a 5 cm × 5 cm model cell. The cell setup taken as FU (Fig. 1) used for the calculations of a laboratory-scale production contains a 100 μm mixed cathode (0.00876 g cm^{-2} LATP and 0.03325 g cm^{-2} NMC 622), a 10 μm LLZO electrolyte layer (0.005107 g cm^{-2}) and a 10 μm lithium film (0.00053 g cm^{-2}). As current collectors 10 μm aluminum (0.0027 g cm^{-2}) and copper films (0.00892 g cm^{-2}) are used. Some results are also shown on a 1 kg basis for ease of comparison, but the large differences in density must be kept in mind. The focus is on the analysis and comparison of the two synthetic routes for LLZO and LATP, as described in Fig. 4.

Table 1 Overview of investigated impact categories

Impact category	Abbreviation	Unit
Climate change, incl biogenic carbon	GWP	kg CO_2 eq.
Fine particulate matter formation	PM	kg PM 2.5 eq.
Fossil depletion	FD	kg oil eq.
Freshwater consumption	Water	m^3
Freshwater ecotoxicity	$ET_{Freshwater}$	kg 1,4 DB eq.
Freshwater eutrophication	$EP_{Freshwater}$	kg P eq.
Human toxicity, cancer	HTP_{cancer}	kg 1,4 DB eq.
Human toxicity, non-cancer	$HTP_{non-cancer}$	kg 1,4 DB eq.
Ionizing radiation	IR	kBq Co-60 eq. to air
Land use	Land	Annual crop eq.·y
Marine ecotoxicity	ET_{Marine}	kg 1,4 DB eq.
Marine eutrophication	EP_{Marine}	kg N eq.
Metal depletion	MD	kg Cu eq.
Photochemical ozone formation, ecosystems	$POCP_{Ecosystems}$	kg NO_x eq.
Photochemical ozone formation, human health	$POCP_{Human\ health}$	kg NO_x eq.
Stratospheric ozone depletion	ODP	kg CFC-11 eq.
Terrestrial acidification	AP	kg SO_2 eq.
Terrestrial ecotoxicity	$ET_{Terrestrial}$	kg 1,4 DB eq.

The assessment follows the cradle-to-gate approach (Fig. 2). All material and energy flows used for the production are included, also the release of emissions on-site. Upstream production and handling processes are considered by using the inventory database Ecoinvent 3.7.1. The air-tight sealing of the battery in an aluminum-coated polyethylene bag is not considered. The usage and recycling phases of the battery pouch are not included in the Life cycle inventory (LCI).

3.1.1 Cell production. The production process of ASB cells by tape casting consists of several different process steps (Fig. 3). The four synthesis pathways for LLZO and LATP are shown in Fig. 4. Most of these processes are currently performed at a laboratory scale. Therefore, the energy and material consumption (Table 2) and the emissions released have not yet been optimized.

The production processes start with the LLZO and LATP powder syntheses, followed by the preparation of the different slurries for the individual components. For the separator slurry, LLZO powder is mixed with organic solvents and additives for dispersing, binding, and plasticizing in a planetary mixer (1200 W) for two minutes. For the mixed-cathode slurry, the prepared LATP powder and NMC 622 are mixed at a weight ratio of 20 : 80. After that, the mixture is processed in the same way as the LLZO powder for the electrolyte slurry above. The energy required for the mixing processes is considered.

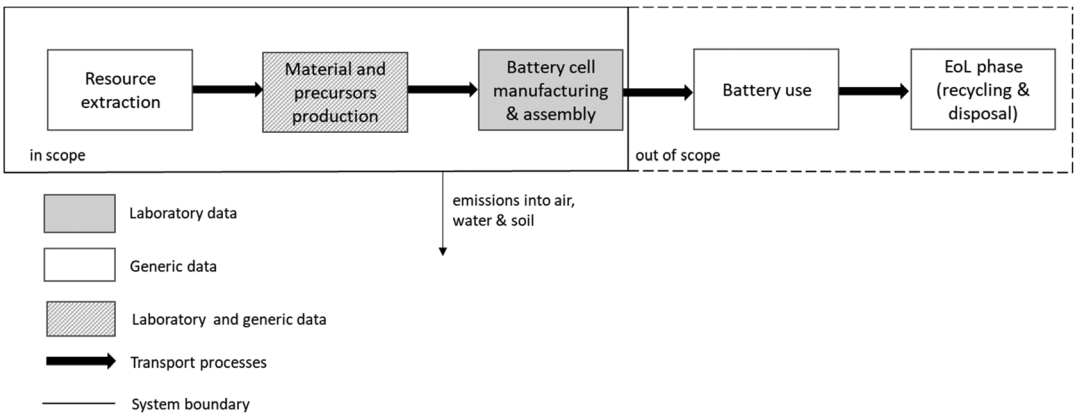

Fig. 2 System boundary of the LCA.

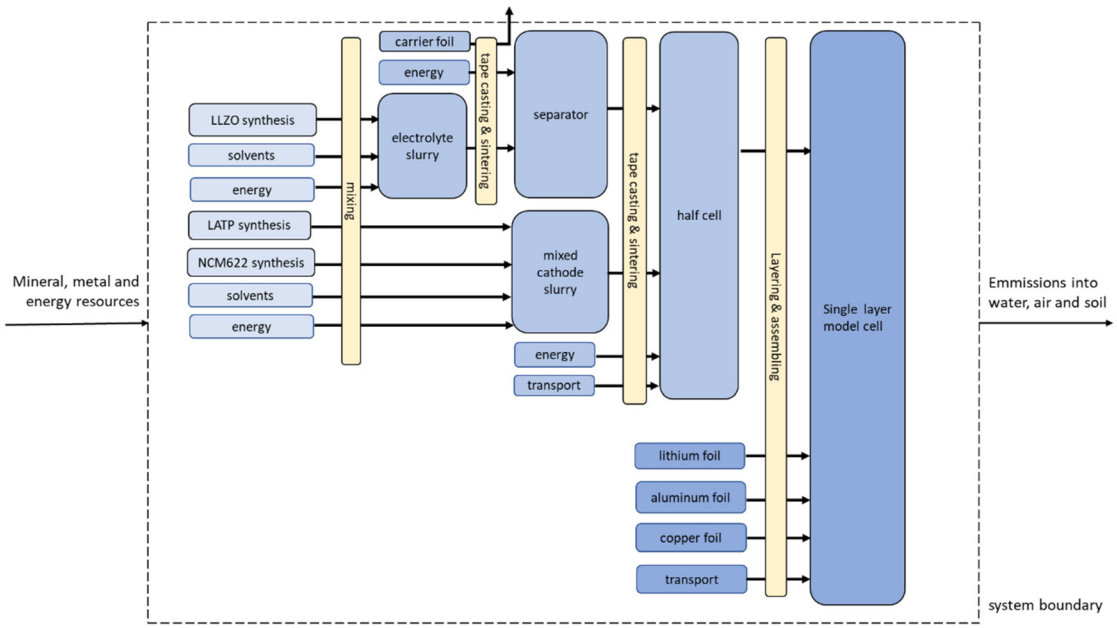

Fig. 3 Flowchart of cell manufacturing adapted and based on ref. 46.

Following the slurry preparation, the different layers of the battery are fabricated using tape casting. First, the pure electrolyte slurry is cast onto a supporting (carrier) PET foil and dried to form a green tape. After its removal from the machine and carrier foil, the green tape is sintered in two subsequent steps (2 h at 650 °C and 2 h at 1150 °C) to produce the separator. Subsequently, the mixed cathode is cast onto the LLZO separator and co-sintered at 650 °C for two hours. The total energy demand is 0.0476 kW per h per 0.05 m^2 for the separator and 0.115 kW per h per 0.05 m^2 for the cathode, including the requirements for mixing, tape casting, and sintering, with 95% of the energy demand being required for sintering. In this idealized process scheme, a 100 μm mixed cathode tightly adhered to a 10 μm electrolyte tape is the result and will be referred to as "half-cell" hereafter. Finally, a half-cell measuring 5 cm by 5 cm is cut out and transferred to a glove box for further processing under argon atmosphere. As an anode, a 10 μm Li metal foil is manually attached to the electrolyte side of the half-cell, creating the full cell. A 10 μm thick Al foil and a 10 μm Cu foil are used as current collectors on the cathode and anode side of the cell, respectively. For the collector foils, we used datasets from the GaBi database ('DE: Aluminium foil Sphera', 'EU-28: copper sheet (A1–A3) Sphera'). For lithium foil, on the other hand, we used an adjusted LCI of a 35 μm thick lithium film published by Deng *et al.*[70]

A 3 wt% increase in the amount of material for the mixed cathode and electrolyte slurry was assumed to compensate for losses during slurry fabrication. In addition, 3 wt% cutting waste was estimated for the different foils and the cell.

Transport of materials *via* lorry were considered throughout all production steps. A synthesis in Germany and an average transport distance of 200 km was assumed.

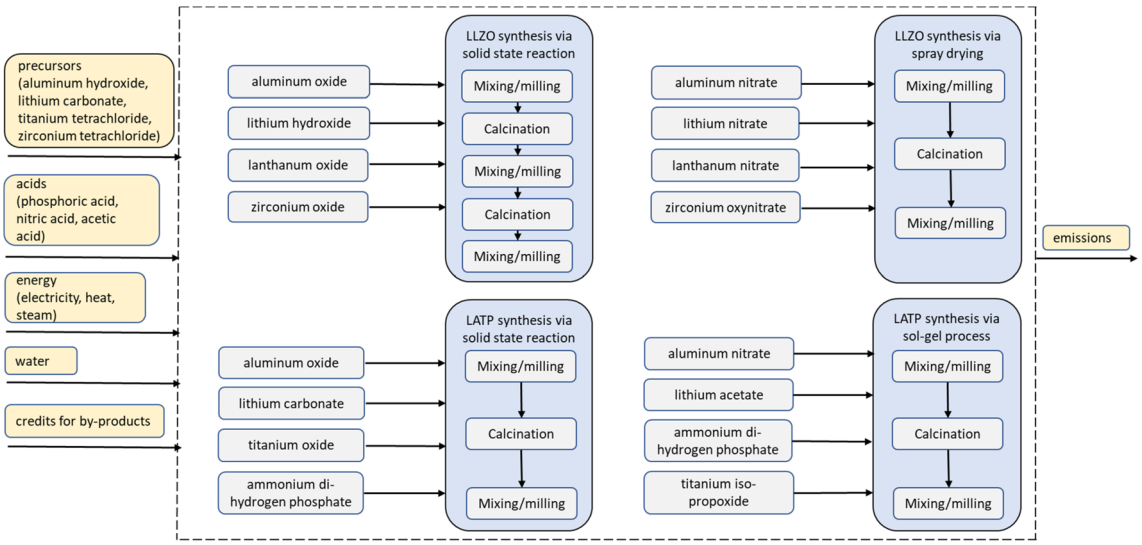

Fig. 4 Materials required for the two synthesis pathways of LLZO and LATP.

Table 2 Materials required for one model cell with 25 cm^2

Material	Quantity	Thickness
Mixed cathode	0.858 g NMC 622 0.226 g LATP	100 μm, 3% offcut
Separator LLZO	0.133 g	10 μm, 3% offcut
Carrier foil (PET)	0.34 g	100 μm, 3% offcut
Li anode	0.0138 g	10 μm, 3% offcut
Al foil	0.0695 g	10 μm, 3% offcut
Cu foil	0.23 g	10 μm, 3% offcut
Argon	0.4 l	
Electricity	0.0281 kW h	

3.1.2 LLZO and LATP synthesis. For comparison, we investigate the synthesis of LLZO using a conventional solid-state reaction as well as a spray drying process. For the solid-state reaction, Al_2O_3, $LiOH{\cdot}H_2O$, La_2O_3 and ZrO_2 are mixed using a mortar grinder. The resulting powder is calcined twice at 850 °C and 1000 °C in an alumina crucible for 20 h. Between each calcination step, the resulting material is milled again. The previously produced metal nitrates or oxynitrates are used for spray drying. Spray drying achieves a fine distribution of the various elements. In addition, as in the solid-state reaction, milling, sieving, and calcination for 1 h at 1000 °C are carried out. Selective catalytic reduction (SCR) with ammonia minimizes the nitrogen oxides produced. After final milling, the LLZO electrolyte powder from both synthesis routes can be used to prepare a slurry for separator casting.

Similarly, LATP is synthesized *via* both a solid-state reaction and a sol–gel process. For the solid-state reaction, Al_2O_3, Li_2CO_3, TiO_2 and $(NH_4)H_2PO_4$ are mixed in a mortar grinder. The resulting powder is milled, calcined for 8 h at 900 °C, and milled again. For the sol–gel process, $Li(CH_3COO){\cdot}2\ H_2O$, $Al(NO_3)_3{\cdot}9\ H_2O$, $(NH_4)H_2PO_4$ and $Ti[OCH(CH_3)_2]_4$ are dissolved in water. After drying, another one hour mixing of the components is required before calcination at 900 °C for 8 h followed by final milling. SCR is performed one more time. After the final milling, the LATP powder from both synthesis routes is mixed with NMC 622 powder and used to prepare a mixed cathode slurry.

The LCI of NMC 622 is from Sun *et al.*,[71] who obtained the information from onsite investigations at two leading cathode material manufacturers in China in 2018, which are among the top five NMC suppliers in the world. The LCI of the required metal components ($NiSO_4$, $MnSO_4$, Li_2CO_3, $LiOH{\cdot}H_2O$) stem from the Ecoinvent 3.7.1 database. For the production of cobalt sulfate, the reaction of cobalt (the data set "cobalt, refined" is from the Cobalt institute and is included in the GaBi database) with sulfuric acid is assumed.

The energy calculations for milling, calcination and spray-drying are described below (Table 3).

A mortar grinder is used for all grinding processes (RM200 Retch, 230 W). The measured energy requirement is 0.19 kW h for a capacity of 200 g. The grinding time is 4 h per grinding step. This results in an energy requirement of 3.8 kW h kg^{-1} of material to be ground. In the calculation of the energy requirement, the powder quantities of individual milling processes are considered. In all process routes, milling takes place after each calcination. In the case of solid-state reaction, additional milling takes place before calcination. The consumption of the grinding balls is not considered. In the sol–gel process, the components are mixed at a rotational speed of 100 rpm for one hour before calcination. Based on the energy of the mortar grinder (400 rpm, 4 h grinding time, 3.8 kW h kg^{-1} powder) and taking into account the shorter grinding time and the lower rotational speed, an energy of 0.24 kW h kg^{-1} capacity was calculated. Considering the quantity of 3.8 kg (2.8 kg LATP powder, 1 kg water), the energy requirement for mixing is 0.9 kW h kg^{-1} LATP powder.

An energy requirement for sieving of 0.1 kW h kg^{-1} is assumed for each process route.

Table 3 Overview of energy requirement per kg LATP or LZZO powder in kW h

Material	Process	Milling	Spray drying	Sieving	Calcination	Sum
LLZO	Spray drying	3.8	7.16	0.10	3.14	14.2
	Solid-state	4.6 (1. milling) 3.8 (2. milling) 3.8 (3. milling)	—	0.10	5.33 (1. calcination) 5.24 (2. calcination)	22.9
LATP	Sol–gel	3.8 0.9 (mixing)	—	0.10	6.9	11.7
	Solid-state	5.8 (1. milling) 3.8 (2. milling)	—	0.10	3.48	12.8

The energy requirement for calcination was measured in a muffle furnace (Nabertherm LT 5/13). Calcination takes place at different temperatures and holding times. The measured energy demand refers to a furnace charge of 3 kg powder. Depending on the starting materials (carbonate, nitrate, oxide), the powder input per kg LLZ or LATP is different.

For the calcination of LATP, the measured energy requirement for preheating and holding is 7.4 kW per h per 3 kg of final LATP powder, 2.8 kg of initial powder is used in the sol–gel route and 1.4 kg in the solid-state route. For the two calcination steps during solid-state synthesis of LLZO, the measured energy requirements for preheating and holding are 13 kW h and 16 kW per h per 3 kg, respectively. The required amount of initial powder is 1.2 kg kg^{-1} final LLZO powder for the first calcination and 1 kg for the second calcination. The spray dryer used can evaporate up to 20 kg of water per hour. At this spray rate, 1 kg of LLZO powder can be processed in about 15 min. Based on the published data by Wittner *et al.*,[72] an energy demand of 7.16 kW h kg^{-1} LLZO was calculated. This includes the energy for heating, atomizing, pump, and ventilator.

For the spray-dried LLZO, the measured energy requirement during calcination for preheating and holding is 4 kW per h per 3 kg. The required amount of nitrate powder kg^{-1} final LLZO powder after spray drying is 2.4 kg, which results in an energy demand of 3.1 kW h. Detailed LCIs of all processes involved can be seen in Tables S1–S23 in the ESI.†

4. Life cycle impact assessment (LCIA)

The results for 18 different impact categories were calculated. Table 4 summarizes them for the different materials used in the model cells (LLZO, LATP, NMC 622) as well as for the liquid electrolyte 1 M $LiPF_6$ dissolved in EC/DMC in the ratio 50 : 50 for comparison with commercial LIBs. With the exception of three impact categories (water consumption, metal depletion, acidification potential), the production of 1 kg LLZO is associated with the highest environmental impacts, followed by the production of 1 kg NMC 622 and 1 kg LATP. While these values are convoluted by the density of the individual materials, with NMC and LLZO being roughly equal (~5 g cm^{-3}), LATP being half this density (~2.3 g cm^{-3}), and the liquid electrolyte the lightest (~1.3 g cm^{-3}), this still gives meaningful insight into the impact of the synthesis method.

Tables 5 and 6 as well as Fig. 8 show that different components of the model cell and steps of the production chain (Fig. 9) have different impacts on the LCA results. The absolute numbers in Fig. 8 and 9 are the same, but the breakdown

Table 4 Absolute LCIA results for different production pathways of 1 kg of LLZO and LATP powders as well as 1 kg of NMC 622 and $LiPF_6$

Impact category	1 kg LLZO solid-state	1 kg LLZO spray drying	1 kg LATP solid-state	1 kg LATP sol–gel	1 kg NMC 622	1 kg LiPF6 (EC/DMC)
WP (kg CO_2 eq.)	37.4	38.9	11.6	15.3	18.2	3.88
PM kg (PM2.5 eq.)	0.054	0.060	0.019	0.012	0.071	0.007
FD (kg oil eq.)	11.9	12.6	3.58	4.79	7.18	1.67
Water consumption (m^3)	0.535	0.606	0.211	0.154	0.733	0.059
ET, freshwater (kg 1,4 DB eq.)	2.02	2.26	0.259	0.155	0.339	0.166
EP, freshwater (kg P eq.)	0.011	0.012	2.8×10^{-3}	2.6×10^{-3}	2.4×10^{-3}	1.3×10^{-3}
HTP, cancer (kg 1,4 DB eq.)	2.75	3	1.3	1.19	0.483	0.301
HTP, non-cancer (kg 1,4 DB eq.)	86.5	97	9.37	7.13	11.3	4.33
IR (kBq Co-60 eq. to air)	3.83	4.22	0.366	0.229	1.15	0.351
Land use (annual crop eq.·y)	7.99	8.63	0.987	0.931	0.905	0.108
ET, marine (kg 1,4 DB eq.)	2.5	2.8	0.337	0.204	0.507	0.209
EP, marine (kg N eq.)	0.301	0.343	7.0×10^{-4}	-3.0×10^{-3}	2.2×10^{-3}	3.6×10^{-4}
Metal depletion (kg Cu eq.)	10.6	11.7	0.569	1.06	12	0.087
POCP, ecosystems (kg NO_x eq.)	0.093	0.101	0.018	0.019	0.036	8.2×10^{-3}
POCP, human Health (kg NO_x eq.)	0.092	0.10	0.018	0.019	0.035	7.9×10^{-3}
ODP (kg CFC-11 eq.)	2.6×10^{-5}	3.8×10^{-5}	5.6×10^{-6}	8.3×10^{-6}	9.7×10^{-6}	1.1×10^{-6}
AP (kg SO_2 eq.)	0.137	0.156	0.^{5}9	0.035	0.237	0.020
ET, terrestrial (kg 1,4 DB eq.)	213	237	19	13.5	190	13.2

Table 5 Total LCIA results for the laboratory scale production of one solid-state battery model cell (LLZO and LATP prepared by solid-state process), together with percentages for different components and process chain parts, the 'energy and waste', 'chemicals & water', and 'transport'

Impact category	Model cell, total	LLZO material (%)	LATP material (%)	NMC 622 material (%)	Li anode material (%)	Chemicals & water (%)	Energy & waste (%)	Trans-port (%)	Carrier foil (%)	Al foil (%)	Cu foil (%)
GWP (kg CO_2 eq.)	0.048	6.9	1.8	16.9	1.4	8.9	58.5	0.2	1.7	1.5	2.2
PM kg (PM2.5 eq.)	8.4×10^{-5}	7.7	4.2	67.6	1.6	4.9	8.7	0.1	0.2	0.6	4.4
FD (kg oil eq.)	0.017	6.5	1.8	17.6	1.3	13.4	53.2	0.2	3.3	1.3	1.5
Water consumption (m^3)	8.9×10^{-4}	7.0	4.4	7.1	1.1	66.5	11.6	0.0	0.5	0.6	1.2
ET, freshwater (kg 1,4 DB eq.)	6.9×10^{-4}	36.7	7.8	38.4	3.4	10.1	3.1	0.2	0.0	0.0	0.3
EP, freshwater (kg P eq.)	4.8×10^{-6}	27.6	11.5	36.6	7.4	14.1	2.5	0.2	0.1	0.0	0.0
HTP, cancer (kg 1,4 DB eq.)	1.2×10^{-3}	24.9	20.0	24.5	4.8	22.5	2.5	0.5	0.0	0.0	0.2
HTP, non-cancer (kg 1,4 DB eq.)	0.027	39.9	7.1	32.3	3.3	8.2	2.8	0.3	0.4	0.1	5.7
IR (kBq Co-60 eq. to air)	2.1×10^{-3}	22.6	2.7	40.9	2.8	7.1	22.7	0.1	0.1	0.9	0.1
Land use (annual crop eq.·y)	3.9×10^{-3}	23.4	2.5	7.4	0.6	5.6	54.9	0.1	0.3	0.3	4.9
ET, Marine (kg 1,4 DB eq.)	9.7×10^{-4}	32.3	7.3	40.8	3.0	9.2	3.6	0.3	0.1	0.0	3.4
EP, marine (kg N eq.)	4.2×10^{-5}	93.0	0.2	3.8	0.4	0.4	2.0	0.0	0.0	0.0	0.1
Metal depletion (kg Cu eq.)	0.012	11.3	1.0	83.1	1.0	0.2	0.4	0.0	0.0	0.0	2.9
POCP, ecosystems (kg NO_x eq.)	2.2×10^{-4}	4.8	1.0	9.8	0.8	3.2	78.3	0.1	0.5	0.5	1.0
POCP, human Health (kg NO_x eq.)	1.6×10^{-4}	6.3	1.4	12.9	1.1	4.1	71.5	0.1	0.6	0.7	1.3
ODP (kg CFC-11 eq.)	$2.4 \times 10^{-0}8$	10.8	1.9	16.6	1.1	8.5	57.6	0.3	0.8	0.5	1.8
AP (kg SO_2 eq.)	2.7×10^{-4}	6.0	4.1	70.3	1.0	4.5	8.7	0.1	0.2	0.6	4.5
ET, terrestrial (kg 1,4 DB eq.)	0.272	10.0	1.3	57.9	0.5	1.7	1.7	0.7	0.8	0.0	25.3

Table 6 Total LCIA results for the laboratory scale production of one solid-state battery model cell (LLZO prepared by spray drying, LATP by sol–gel process), together with percentages for different components and process chain parts, the 'energy and waste', 'chemicals & water', and 'transport'

Impact category	Model cell, total	LLZO material (%)	LATP material (%)	NMC 622 material (%)	Li (%) anode material	Chemicals & water (%)	Energy & waste (%)	Trans-port (%)	Carrier foil (%)	Al foil (%)	Cu foil (%)
GWP (kg CO_2 eq.)	0.049	7.4	2.9	16.8	1.4	8.6	57.4	0.2	1.7	1.5	2.1
PM kg (PM2.5 eq.)	8.4×10^{-5}	8.6	3.3	69.4	1.6	2.3	9.3	0.1	0.3	0.6	4.5
FD (kg oil eq.)	0.017	7.0	3.7	17.4	1.3	12.4	52.0	0.2	3.3	1.3	1.5
Water consumption (m^3)	8.8×10^{-4}	8.0	4.0	7.4	1.1	64.9	12.2	0.0	0.5	0.7	1.3
ET, freshwater (kg 1,4 DB eq.)	7.0×10^{-4}	42.3	7.3	39.9	3.5	2.7	3.8	0.2	0.1	0.0	0.3
EP, freshwater (kg P eq.)	4.9×10^{-6}	31.1	14.3	38.5	7.8	4.1	3.8	0.2	0.1	0.0	0.0
HTP, cancer (kg 1,4 DB eq.)	1.2×10^{-3}	31.8	24.1	29.2	5.7	4.5	3.7	0.5	0.1	0.0	0.3
HTP, non-cancer (kg 1,4 DB eq.)	0.028	45.0	7.1	32.7	3.3	2.0	3.3	0.3	0.5	0.1	5.8
IR (kBq Co-60 eq. to air)	2.1×10^{-3}	25.2	2.3	40.7	2.8	5.5	22.2	0.1	0.1	0.9	0.1
Land use (annual crop eq.·y)	3.9×10^{-3}	26.5	2.5	7.5	0.6	3.7	53.7	0.1	0.3	0.3	4.9
ET, marine (kg 1,4 DB eq.)	9.8×10^{-4}	37.2	6.7	42.4	3.1	2.5	4.2	0.3	0.1	0.0	3.5
EP, marine (kg N eq.)	4.7×10^{-5}	95.5	0.2	3.4	0.3	-1.4	1.8	0.0	0.0	0.0	0.1
Metal depletion (kg Cu eq.)	0.013	12.2	1.9	81.5	1.0	0.1	0.5	0.0	0.0	0.0	2.9
POCP, ecosystems (kg NO_x eq.)	2.2×10^{-4}	12.3	1.5	68.2	0.8	2.6	12.5	0.1	0.5	0.5	1.0
POCP, human Health (kg NO_x eq.)	1.7×10^{-4}	12.8	1.9	61.6	1.1	3.3	16.7	0.1	0.6	0.7	1.3
ODP (kg CFC-11 eq.)	$2.6 \times 10^{-0}8$	11.2	2.6	15.4	1.0	14.2	52.4	0.3	0.8	0.5	1.7
AP (kg SO_2 eq.)	2.7×10^{-4}	6.8	2.7	72.2	1.0	2.2	9.6	0.1	0.3	0.6	4.6
ET, terrestrial (kg 1,4 DB eq.)	0.275	11.2	1.2	57.9	0.5	0.6	1.8	0.6	0.9	0.0	25.3

either in components or upstream steps is different. The columns and bars "Energy & waste", "Chemicals & water", and "Transport" (Tables 5, 6 and Fig. 9) are cumulative values for individual energy demands, chemical (*e.g.*, solvents, additives for dispersing, binding) and water supplies, waste treatment, and transport along the entire process chain. It describes the overall consumption of electricity, chemicals, water *etc*. in the laboratory during the production of the composite cathode, the electrolyte, and the assembly of the model cell, but not the electricity consumption, *etc*. during the production of the purchased products (Al foil, Cu foil).

The use of La_2O_3 and $La(NO_3)_3{\cdot}6H_2O$ results in the increased impacts for LLZO (Fig. 5 and 6), with the supply of lanthanum as one of the critical raw materials listed in 2020.[73] The energy demand required during the production of LATP causes the highest GWP and FD, followed by the supply of Ti$[OCH(CH_3)_2]_4$, $[Li(CH_3COO){\cdot}2H_2O]$, TiO_2, and $(NH_4)H_2PO_4$ (Fig. 5 and 6). However, the supply of $(NH_4)H_2PO_4$ causes the highest environmental impacts for the most categories. This result is in accordance with the latest literature,[53] in which also the LATP precursors have a significant influence on LATP synthesis.

There is little difference in the environmental impacts of the different synthesis routes, which true for both LLZO and LATP powders (Fig. 5 and 6). LLZO produced by spray drying has 4 to 12% higher environmental impacts than LLZO produced by solid-state reaction, which is negligible within the data uncertainties. Only for ODP, the difference is 32% (Table 4). LATP powder produced by solid-state reaction has higher environmental impacts in 12 of 18 categories (Table 4). The accounting of NH_4Cl co-production in Ti$[OCH(CH_3)_2]_4$ production is the cause of a negative EP_{Marine} potential (Table 4).

Since the environmental impacts of the different synthesis methods are low at the scale studied, the selection of the most suitable method for industrial scale application depends mainly on the energy consumption of the larger scale production plants, as well as on the use and recycling of the additives.

The environmental impact of the cathode active material NMC 622 (Fig. 5 and 6) can be reduced in future cell designs, as suggested by Winjobi *et al.*[74] By reducing cobalt content significantly in favor of nickel, which has a lower environmental impact, the total energy impact of NMC can be improved while simultaneously increasing the energy density.

Comparing the above materials on a 1 kg of powder basis with the liquid electrolyte $LiPF_6$ used in conventional lithium-ion batteries, the liquid electrolyte performs best, as expected (Fig. 5 and 6). Only IR and ET_{Marine} are slightly lower for 1 kg LATP (sol–gel). However, in a battery cell, which represented by the model cell in this study, the materials have vastly different shares of the overall mass. In addition, the influence of component production must also be considered.

Therefore, the more meaningful comparison is the cumulative impact on the cell level (Tables 5 and 6, Fig. 8 and 9), using the respective values defined for our model cell (Table 2).

At the model cell level, the impact of NMC 622 and the energy consumption of synthesis and component manufacturing dominate the environmental impact in all categories. The

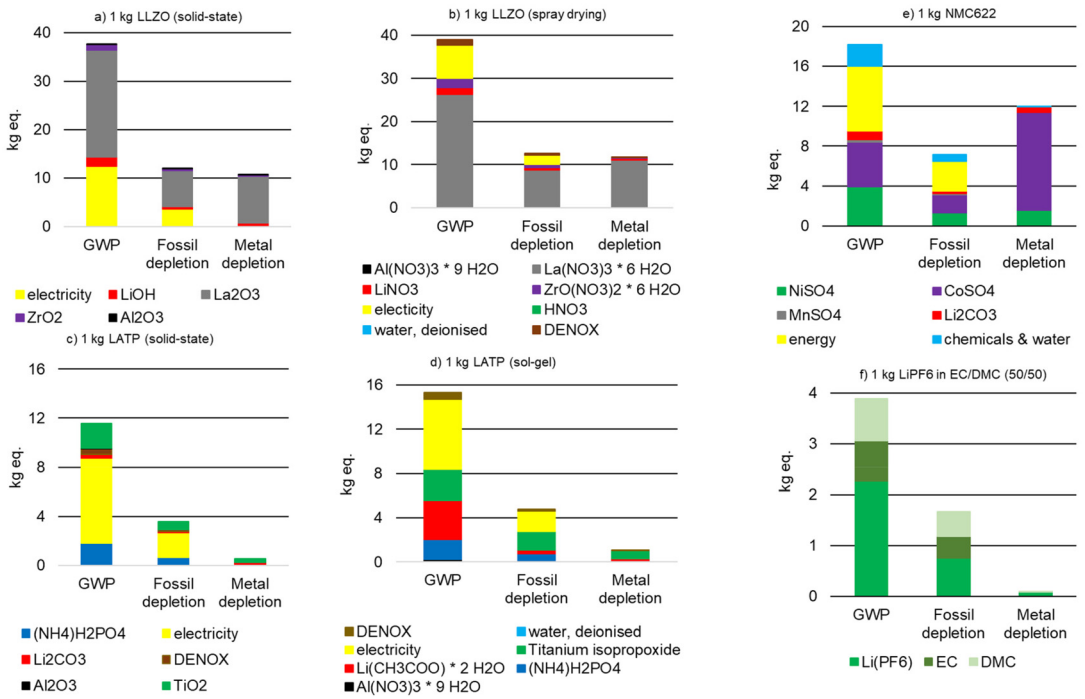

Fig. 5 GWP, fossil depletion and metal depletion of (a) of 1 kg of LLZO (solid-state), (b) 1 kg of LLZO (spray drying), (c) 1 kg of LATP (solid-state), (d) 1 kg of LATP (sol–gel), (e) 1 kg of NMC 622, (f) 1 kg of LiP_6 in EC/DMC 50/50.

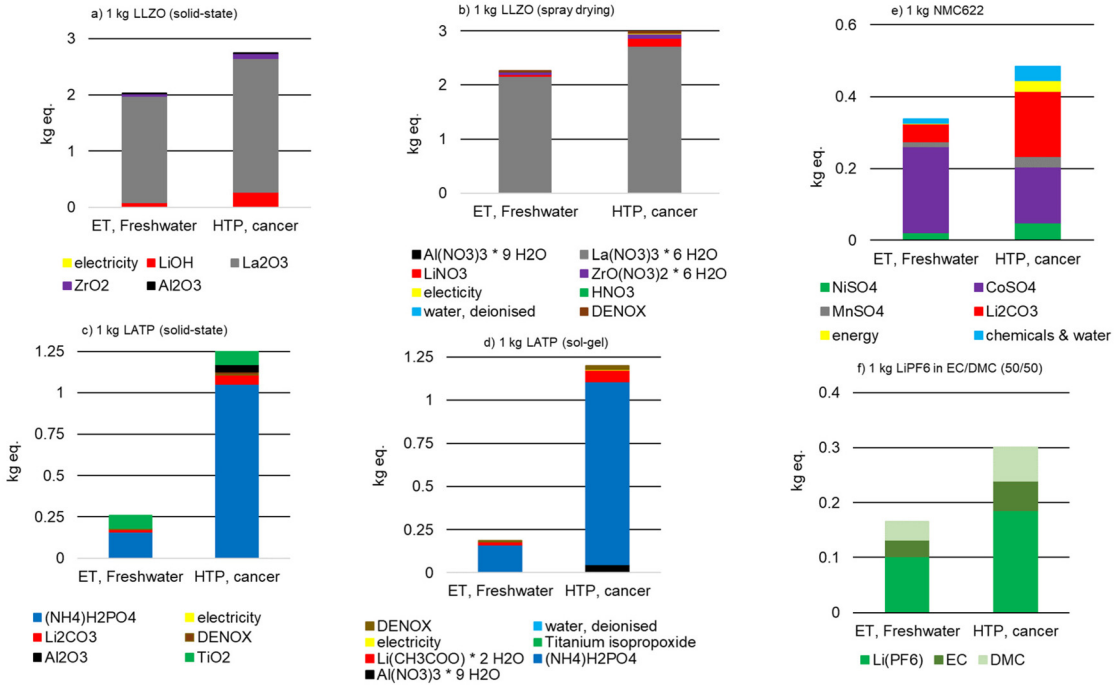

Fig. 6 ET, freshwater and HTP, cancer of (a) of 1 kg of LLZO (solid-state), (b) 1 kg of LLZO (spray drying), (c) 1 kg of LATP (solid-state), (d) 1 kg of LATP (sol–gel), (e) 1 kg of NMC 622, (f) 1 kg of LiP_6 in EC/DMC 50/50.

pie chart (Fig. 7) shows the energy demand in detail. The total energy resources amount to 1.08 MJ for the model cell. In the case of the mixed cathode (52% share of the total model cell), 88% of the energy is used for the production of powder and cathode slurry, and only 12% for tape casting and sintering of the cathode. A significant share of the energy consumption (30% of the total energy consumption) is attributed to the process of cell assembly in a glovebox. It was assumed that only one cell per workstation can be produced at a time in a laboratory glovebox. In this case, a glovebox with three workstations was used as a benchmark. On an industrial scale, it can be assumed that this can be done much more efficiently

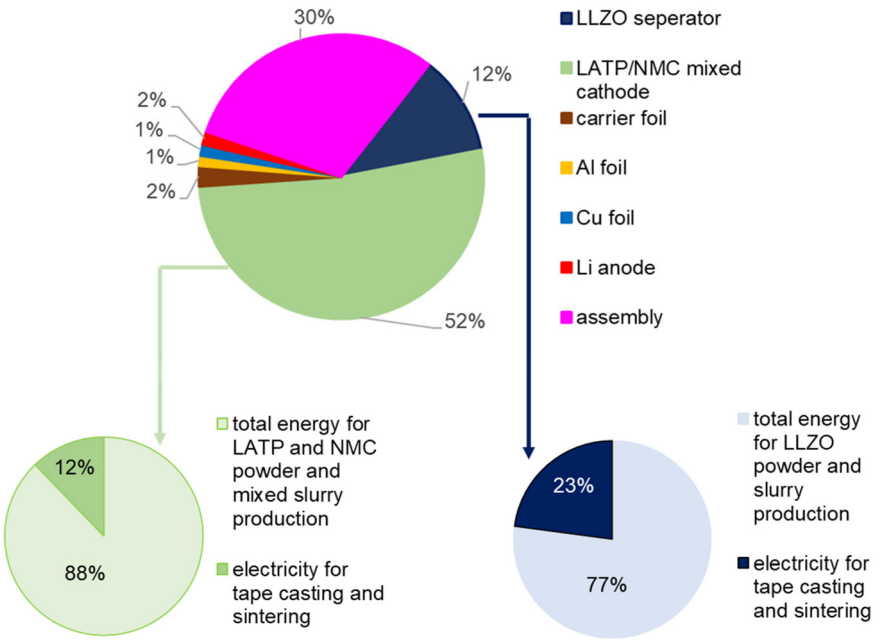

Fig. 7 Share of cell components on the overall energy demand of 1 model cell (LLZ/LATP solid-state reaction).

and that several cells can be produced simultaneously, so that the energy requirement per cell can be greatly reduced. In the case of the LLZO separator (12% share of the total model cell), 77% of the energy resources are required for LLZO powder and slurry synthesis and 23% for the power requirements for sintering and tape casting.

Since energy consumption plays a major role in the environmental impact of the cell, there is great potential for improvement. In this study, batch synthesis of electrolytes on a one-kilogram scale and small-scale fabrication of 5 cm × 5 cm components and cells were investigated. Nevertheless, all processing steps were carefully chosen for their scalability. Therefore, a significant reduction in energy consumption per cell can be expected when the entire process chain is scaled up to industrially relevant levels.

The influence of the pouch case material and welding is negligible and is only reduced when upscaling to multilayer cells, so it was not considered in this study. While the content of NMC 622 cannot be reduced, as it is the cathode active material, clear pathways for future cell design improvements can be derived from these findings. Since LATP has a much lower environmental impact than LLZO, it is the right choice as the electrolyte material for the mixed cathode. Nevertheless, the design of the mixed cathode should be further optimized to reduce the LATP content while increasing the thickness of the mixed cathodes to increase the overall NMC 622 content in the model cell. As already mentioned in Zhang,[53] the thickness of LATP and the energy-intensive manufacturing processes of LATP are among the main factors for environmental pollution. A switch to NMC 811, which has an even lower cobalt content than NMC622 may also help to further reduce the environmental impact of the mixed cathode at the cell level. It should be reiterated that these suggestions represent the overall goal for design optimization and that the practical implementation of this approach has yet to be demonstrated. In particular, suppression of secondary phase formation during sintering and improvement of cycling stability of the cathodes are still current research challenges that may require the use of additives or protective coatings, which were not considered in this study. LLZO is required as an electrolyte and separator to enable the use of a lithium metal anode, but its environmental impact is twice as high in all categories. Therefore, future optimized cell designs should aim to further reduce the thickness of the separator *e.g.*, by using PVD or sol–gel thin film processes that can cut the thickness at least in half. Although the environmental impact of ceramic solid-state lithium batteries is still higher than the impact of conventional lithium-ion batteries at the current development level, we have demonstrated the plausibility of the cell design studied.

Fig. 8 and 9 show the same absolute environmental impacts of the elements of the model cells summarized in different ways, with Fig. 8 subdivided by cell components and Fig. 9 subdivided by materials and upstream processes. An expected result from Fig. 8 is that the mixed cathode is the largest contributor to the impact generated, with the use of NMC 622 being the largest contributor. Energy supply is the main contributor to GWP and fossil depletion (Fig. 9), followed by the material supply required for NMC 622 production, whose environmental impact is clearly visible in all environmental categories shown. In the case of HTP_{cancer}, LATP, LLZO

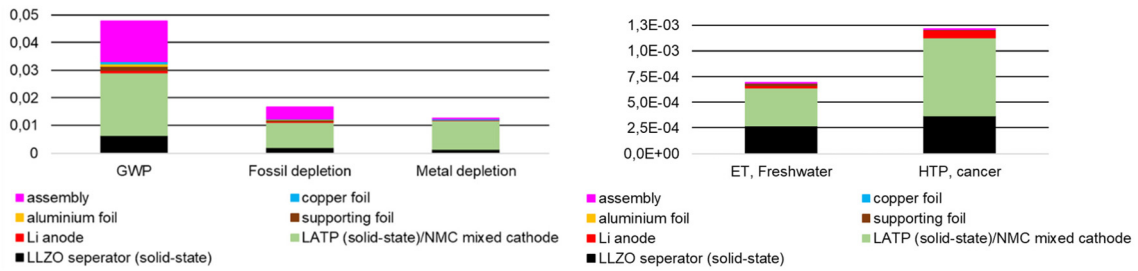

Fig. 8 Environmental impacts of 1 model cell divided according to cell components ((LLZ/LATP solid-state reaction).

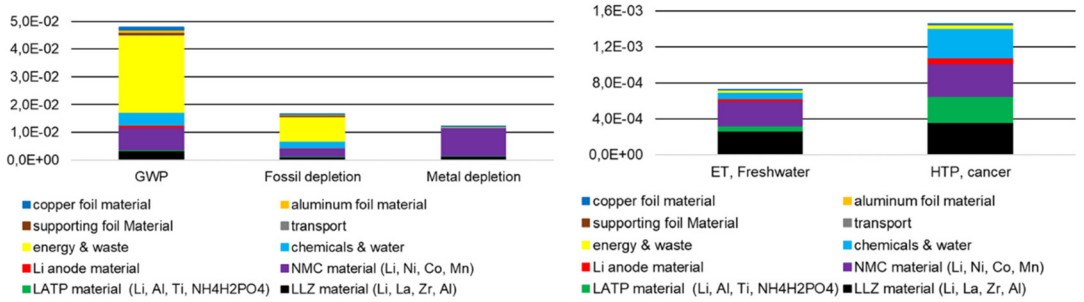

Fig. 9 Environmental impacts of 1 model cell divided according to materials and up-stream processes (LLZ/LATP solid-state reaction).

and the chemicals also significant contributions (Fig. 9). The GWP of 0.048 kg CO_2 eq. per model cell corresponds to approx. 31 kg CO_2 eq. kg^{-1} battery and is in a similar order of magnitude to the GWP of 23 kg CO_2 eq. kg^{-1} battery, as calculated by Pell and Lindsay.[54] However, compared to this LCA, the latter does not include transportation impacts, energy inputs for creating the argon atmosphere required for ASB electrode/electrolyte assembly, and energy inputs for precursor material (powder and slurry production). The results given for AP, ODP, POCP, and EP (Table 5) as well as for the total energy demand are in the same order of magnitude given for batteries with NMC chemistry shown in the study of Arshad *et al.*[56]

Aluminum, copper, the carrier foil and the lithium anode as well as all transports have rather low impacts in most categories (Tables 5 and 6). Most of them are below 1%, a few between 1% and 8%. Chemical supply & water only have a notable impact in the water consumption category at about 65%. Energy & waste supply are the main contributors for four impact categories (GWP, FD, Land use, ODP). The supply of materials needed for production of NMC 622 causes the highest values in 8 out of 18 impact categories. The material supply for LLZO production has the highest impacts for $ET_{Freshwater}$, HTP_{cancer}, $HTP_{non-cancer}$, and EP_{Marine} (95% of the total impact). The high share of EP_{Marine} impact is due to the supply of $La_2(NO_3)_3$.

A comparison of the materials required for one model cell with another model cell consisting of an equivalent quantity of $LiPF_6$ (in EC/DCM), which could theoretically replace LATP and LLZO can be found in the ESI (Fig. S1†). The comparison is based on the different densities of the materials put into ratio.

5. Conclusions

In our study, we evaluated the environmental impact of manufacturing an all-solid-state battery with tailored oxide-based solid electrolytes for cathode and separator. With respect to cost-cutting aspects, we defined a reasonable cell design that is close to the state of the art and combines the advantages of LLZO as separator and LATP as electrolyte in the mixed all-solid-state cathode. All steps from material synthesis to scalable cell fabrication process were investigated, including all material and energy inputs as well as the emissions and waste materials. In particular, for the solution-based synthesis of the LLZO and LATP electrolytes, the nitrogen oxide emission was considered. The LCA results lead to several valuable insights for the future optimization of oxide-based ASBs.

First, the comparison of electrolytes prepared by different synthesis methods shows no significant advantage of either method within the investigated batch size. Therefore, the choice of synthesis method for LLZO and LATP can be reasonably made based on economic criteria if the materials are to be produced on an industrial scale. Of the two materials, LATP has a much lower environmental impact than LLZO, further validating the proposed cell concept which was based on performance and cost considerations and synergistically combines the advantages of both materials.

Second, the overall fabrication process of a single model cell was examined and revealed several points for future improvement. While the largest contribution for most categories came from the synthesis of NMC 622 cathode active material, the second largest contribution was energy consumption during full cell assembly in inert atmosphere. Careful upscaling and automation of the lithium metal anode application and full cell assembly processes in industrial application can significantly reduce both the energy cost and the environmental impact. Further optimizations to the processing chain can include novel ceramic processing techniques such as FAST/SPS and aerosol deposition (AD), or the switch from NMC 622 to 811 or even higher Ni-containing cathode active materials with significantly enhanced energy density can further reduce the environmental impact.

The clear roadmap for economic and environmental feasibility is therefore to realize a similar cell concept using scalable ceramic manufacturing routes, especially focusing on new, energy-saving sintering technologies and optimized cathode active materials that take full advantage of non-liquid electrolytes.

Overall, effort to further reduce the environmental impact of solid-state batteries production face the same challenges as those faced in conventional lithium-ion battery manufacturing years ago: dominant influence of the cathode active material, need to optimize electrolyte content, and reduction of energy consumption during manufacturing steps. Nevertheless, the results of our investigation place the impact of oxide-based solid-state electrolytes in all-solid-state battery manufacturing on the same order of magnitude as conventional lithium-ion batteries with liquid electrolytes. This solid foundation provides a positive future perspective for the development of competitive oxide-based all-solid-state lithium batteries.

Author contributions

A. S. and M. R. contributed equally to this work; A. S. performed the life cycle assessment, investigation, methodology, writing – original draft, visualization; M. R. data collection, validation, visualization, writing – conceptualization, original draft; K. W. data collection, writing – review & editing; K. N. supervision, writing – review & editing; N. S.: data collection, writing – original draft; H. W. supervision, writing – review & editing; M. K. data collection, validation; D. F.-R. funding acquisition, supervision, writing – review & editing; W. K. supervision, writing – review & editing; O. G. funding acquisition, supervision, writing – review & editing; M. F. conceptualization, writing – original draft, funding acquisition, project administration, supervision.

Conflicts of interest

There are no conflicts to declare.

Acknowledgements

Financial support from the German Federal Ministry of Education and Research BMBF within the Project EProFest (13XP0346B) and the clusters of competency Festbatt-Oxide (13XP0173A/03XP0173D), Festbatt2-Oxide (13XP0434A, 03XP0434B) and FestBatt2-Production (13XP0432, 03XP0432E) is gratefully acknowledged. Financial support is also acknowledged from the Helmholtz foundation, Program MTET, Topic 2. The authors would like to thank Michael Küpers and Grit Häuschen from IEK-1 for the help with data acquisition regarding electrolyte synthesis and component sintering and Jean Philippe Beaupain, Mareike Partsch and Mihails Kusnezoff from Fraunhofer IKTS for fruitful discussions regarding composite cathode and cell manufacturing.

References

1 B. A. L. Robinson, Solid-state Batteries Enter EV Fray, *MRS Bull.*, 2014, 1046–1047.
2 J. B. Goodenough and Y. Kim, Challenges for Rechargeable Li Batteries, *Chem. Mater.*, 2010, 587–603.
3 S. Li, F. Lorandi, H. Wang, T. Liu, J. F. Whitacre and K. Matyjaszewski, Functional polymers for lithium metal batteries, *Prog. Polym. Sci.*, 2021, 101453.
4 X. Yang, M. Jiang, X. Gao, D. Bao, Q. Sun, N. Holmes, *et al.*, Determining the limiting factor of the electrochemical stability window for PEO-based solid polymer electrolytes: Main chain or terminal -OH group?, *Energy Environ. Sci.*, 2020, 1318–1325.
5 Q. Li, H. Y. Sun, Y. Takeda, N. Imanishi, J. Yang and O. Yamamoto, Interface properties between a lithium metal electrode and a poly(ethylene oxide) based composite polymer electrolyte, *J. Power Sources*, 2001, 201–205.
6 N. A. Stolwijk, C. Heddier, M. Reschke, M. Wiencierz, J. Bokeloh and G. Wilde, Salt-Concentration Dependence of the Glass Transition Temperature in PEO – NaI and PEO – LiTFSI Polymer Electrolytes, *Macromolecules*, 2013, 8580–8588.
7 R. J. Chen, Y. B. Zhang, T. Liu, B. Q. Xu, Y. H. Lin, C. W. Nan, *et al.*,Addressing the Interface Issues in All-Solid-State Bulk-Type Lithium Ion Battery via an All-Composite Approach, *ACS Appl. Mater. Interfaces*, 2017, 9654–9661.
8 Y. Kato, S. Hori, T. Saito, K. Suzuki, M. Hirayama, A. Mitsui, *et al.*,High-power all-solid-state batteries using sulfide superionic conductors, *Nat. Energy*, 2016, 16030.
9 X. Yao, D. Liu, C. Wang, P. Long, G. Peng, Y. S. Hu, *et al.*, High-Energy All-Solid-State Lithium Batteries with Ultralong Cycle Life, *Nano Lett.*, 2016, 7148–7154.
10 486 S. Pierce Ave. SELC 80027 (HQ)., and 14902 Grant Street U 120–140 TC 80023., *Solid Power*.
11 R. Koerver, W. Zhang, L. de Biasi, S. Schweidler, A. O. Kondrakov, S. Kolling, *et al.*,Chemo-mechanical expansion of lithium electrode materials – on the route to mechanically optimized all-solid-state batteries, *Energy Environ. Sci.*, 2018, 2142–2158.
12 B. Neudecker, N. J. Dudney and J. B. Bates, Lithium-Free" Thin-Film Battery with In Situ Plated Li Anode B., *J. Electrochem. Soc.*, 2000, **147**, 517–523.
13 R. DeWees and H. Wang, Synthesis and Properties of NaSICON-type LATP and LAGP Solid Electrolytes, *ChemSusChem*, 2019, 3713–3725.
14 B. Davaasuren and F. Tietz, Impact of sintering temperature on phase formation, microstructure, crystallinity and ionic conductivity of Li1.5Al0.5Ti1.5(PO4)3, *Solid State Ionics*, 2019, 144–152.
15 P. Birke, F. Salam, S. Döring and W. Weppner, A first approach to a monolithic all solid state inorganic lithium battery, *Solid State Ionics*, 1999, 149–157.
16 L. Miara, A. Windmüller, C. L. Tsai, W. D. Richards, Q. Ma, S. Uhlenbruck, *et al.*,About the Compatibility between High Voltage Spinel Cathode Materials and Solid Oxide Electrolytes as a Function of Temperature, *ACS Appl. Mater. Interfaces*, 2016, 26842–26850.
17 T. Kato, S. Iwasaki, Y. Ishii, M. Motoyama, W. C. West, Y. Yamamoto, *et al.*,Preparation of thick-film electrode-solid electrolyte composites on Li7La3Zr2O12 and their electrochemical properties, *J. Power Sources*, 2016, 65–72.
18 A. Sharafi, E. Kazyak, A. L. Davis, S. Yu, T. Thompson, D. J. Siegel, *et al.*,Surface Chemistry Mechanism of Ultra-Low Interfacial Resistance in the Solid-State Electrolyte Li7La3Zr2O12, *Chem. Mater.*, 2017, 7961–7968.
19 C. Bernuy-Lopez, W. Manalastas, J. M. Lopez Del Amo, A. Aguadero, F. Aguesse and J. A. Kilner, Atmosphere controlled processing of ga-substituted garnets for high li-ion conductivity ceramics, *Chem. Mater.*, 2014, 3610–3617.
20 M. Rosen, R. Ye, M. Mann, S. Lobe, M. Finsterbusch, O. Guillon, *et al.*,Controlling the lithium proton exchange of LLZO to enable reproducible processing and performance optimization, *J. Mater. Chem. A*, 2021, 4831–4840.
21 M. Finsterbusch, T. Danner, C. L. Tsai, S. Uhlenbruck, A. Latz and O. Guillon, High Capacity Garnet-Based All-Solid-State Lithium Batteries: Fabrication and 3D-Microstructure Resolved Modeling, *ACS Appl. Mater. Interfaces*, 2018, 22329–22339.
22 E. Rangasamy, J. Wolfenstine and J. Sakamoto, The role of Al and Li concentration on the formation of cubic garnet solid electrolyte of nominal composition Li 7La 3Zr 2O 12, *Solid State Ionics*, 2012, 28–32.
23 Y. Jin and P. J. McGinn, Al-doped Li7La3Zr2O12 synthesized by a polymerized complex method, *J. Power Sources*, 2011, 8683–8687.
24 E. Zhao, F. Ma, Y. Jin and K. Kanamura, Pechini synthesis of high ionic conductivity Li1.3Al0.3Ti1.7 (PO4)3 solid electrolytes: The effect of dispersant, *J. Alloys Compd.*, 2016, 646–653.
25 X. Xu, Z. Wen, J. Wu and X. Yang, Preparation and electrical properties of NASICON-type structured Li1.4Al0.4Ti1.6 (PO4)3 glass-ceramics by the citric acid-assisted sol-gel method, *Solid State Ionics*, 2007, 29–34.

26 F. Langer, J. Glenneberg, I. Bardenhagen and R. Kun, Synthesis of single phase cubic Al-substituted Li7La3Zr2O12 by solid state lithiation of mixed hydroxides, *J. Alloys Compd.*, 2015, 64–69.
27 E. Yi, W. Wang, J. Kieffer and R. M. Laine, Key parameters governing the densification of cubic-Li7La3Zr2O12Li+ conductors, *J. Power Sources*, 2017, 156–164.
28 K. Waetzig, A. Rost, C. Heubner, M. Coeler, K. Nikolowski, M. Wolter, *et al.*,Synthesis and sintering of Li1.3Al0.3Ti1.7 (PO4)3 (LATP) electrolyte for ceramics with improved Li+ conductivity, *J. Alloys Compd.*, 2020, 153237.
29 M. Mann, M. Küpers, G. Häuschen, M. Finsterbusch, D. Fattakhova-Rohlfing and O. Guillon, Evaluation of scalable synthesis methods for aluminum-substituted li7la3zr2o12 solid electrolytes, *Materials*, 2021, 1–16.
30 L. Schwich, M. Küpers, M. Finsterbusch, A. Schreiber, D. Fattakhova-Rohlfing, O. Guillon, *et al.*,Recycling strategies for ceramic all-solid-state batteries—part i: Study on possible treatments in contrast to li-ion battery recycling, *Metals*, 2020, 1–19.
31 L. Azhari, S. Bong, X. Ma and Y. Wang, Recycling for All Solid-State Lithium-Ion Batteries, *Matter*, 2020, 1845–1861.
32 M. A. Rajaeifar, M. Raugei, B. Steubing, A. Hartwell, P. A. Anderson and O. Heidrich, Life cycle assessment of lithium-ion battery recycling using pyrometallurgical technologies, *J. Ind. Ecol.*, 2021, 1560–1571.
33 J. F. Peters, M. Baumann, B. Zimmermann, J. Braun and M. Weil, The environmental impact of Li-Ion batteries and the role of key parameters–A review, *Renewable Sustainable Energy Rev.*, 2017, 491–506.
34 D. A. Notter, M. Gauch, R. Widmer, P. Wäger, A. Stamp, R. Zah, *et al.*,Erratum: Contribution of li-ion batteries to the environmental impact of electric vehicles (Environmental Science & Technology (2010) 44 (6550–6556)), *Environ. Sci. Technol.*, 2010, 7744.
35 G. Majeau-Bettez, T. R. Hawkins and A. H. Strømman, Erratum: Life cycle environmental assessment of lithium-ion and nickel metal hydride batteries for plug-in hybrid and battery electric vehicles, *Environ. Sci. Technol.*, 2011, 5454.
36 J. B. Dunn, L. Gaines, J. C. Kelly, C. James and K. G. Gallagher, The significance of Li-ion batteries in electric vehicle life-cycle energy and emissions and recycling's role in its reduction, *Energy Environ. Sci.*, 2015, 158–168.
37 L. A. W. Ellingsen, G. Majeau-Bettez, B. Singh, A. K. Srivastava, L. O. Valøen and A. H. Strømman, Life Cycle Assessment of a Lithium-Ion Battery Vehicle Pack, *J. Ind. Ecol.*, 2014, 113–124.
38 M. Erakca, M. Baumann, W. Bauer, L. de Biasi, J. Hofmann, B. Bold, *et al.*,Energy flow analysis of laboratory scale lithium-ion battery cell production, *iScience.*, 2021, 102437.
39 J. F. Peters and M. Weil, Providing a common base for life cycle assessments of Li-Ion batteries, *J. Cleaner Prod.*, 2018, 704–713.
40 Q. Dai, J. Kelly, J. Dunn and P. Benavides, Update of Bill-of-Materials and Cathode Materials Production for Lithium-Ion Batteries in the GREET Model, in *Energy Systems Division: Argonne National Laboratory (ANL), IL, US*, Energy Systems Division: Argonne National Laboratory (ANL), IL, US, 2018.
41 Q. Dai, J. C. Kelly, L. Gaines and M. Wang, Life cycle analysis of lithium-ion batteries for automotive applications, *Batteries*, 2019, 48.
42 N. B. Manjong, L. Usai, O. S. Burheim and A. H. Strømman, Life cycle modelling of extraction and processing of battery minerals—a parametric approach, *Batteries*, 2021, 57.
43 L. A. W. Ellingsen, C. R. Hung and A. H. Strømman, Identifying key assumptions and differences in life cycle assessment studies of lithium-ion traction batteries with focus on greenhouse gas emissions, *Transp. Res. Part D Transp. Environ.*, 2017, 82–90.
44 E. Crenna, M. Gauch, R. Widmer, P. Wäger and R. Hischier, Towards more flexibility and transparency in life cycle inventories for Lithium-ion batteries, *Resour., Conserv. Recycl.*, 2021, 15619.
45 M. Chordia, A. Nordelöf and L. A. W. Ellingsen, Environmental life cycle implications of upscaling lithium-ion battery production, *Int. J. Life Cycle Assess.*, 2021, 2024–2039.
46 C. M. Lastoskie and Q. Dai, Comparative life cycle assessment of laminated and vacuum vapor-deposited thin film solid-state batteries, *J. Cleaner Prod.*, 2015, 158–169.
47 S. Troy, A. Schreiber, T. Reppert, H.-G. Gehrke, M. Finsterbusch, S. Uhlenbruck, *et al.*,Life Cycle Assessment and resource analysis of all-solid-state batteries, *Appl. Energy*, 2016, 757–767.
48 A. Keshavarzmohammadian, S. M. Cook and J. B. Milford, Cradle-to-gate environmental impacts of sulfur-based solid-state lithium batteries for electric vehicle applications, *J. Cleaner Prod.*, 2018, 770–778.
49 F. Rossi, M. L. Parisi, S. Greven, R. Basosi and A. Sinicropi, Life cycle assessment of classic and innovative batteries for solar home systems in Europe, *Energies*, 2020, 3454.
50 M. Zackrisson, L. Avellán and J. Orlenius, Life cycle assessment of lithium-ion batteries for plug-in hybrid electric vehicles - Critical issues, *J. Cleaner Prod.*, 2010, 1517–1527.
51 C. Bauer, *Ökobilanz von Lithium-Ionen Batterien*, Paul Scherrer Institut, Labor für Energiesystem-Analysen (LEA), Villingen, Switz., 2010.
52 L. Smith, T. Ibn-Mohammed, D. Astudillo, S. Brown, I. M. Reaney and S. C. L. Koh, The Role of Cycle Life on the Environmental Impact of Li6.4La3Zr1.4Ta0.6O12 based Solid-State Batteries, *Adv. Sustainable Syst.*, 2021, 2000241.
53 J. Zhang, X. Ke, Y. Gu, F. Wang, D. Zheng, K. Shen, *et al.*, Cradle-to-gate life cycle assessment of all-solid-state lithium-ion batteries for sustainable design and manufacturing, *Int. J. Life Cycle Assess.*, 2022, 227–237.

54 R. Pell and J. J. Lindsay, *Comparative life cycle assessment study of solid state and lithium-ion batteries for electric vehicle application in*, 2022.
55 M. Salado, E. Lizundia, I. Oyarzabal and D. Salazar, The Role of Critical Raw Materials for Novel Strategies in Sustainable Secondary Batteries, *Phys. Status Solidi A*, 2022, 2100710.
56 F. Arshad, J. Lin, N. Manurkar, E. Fan, A. Ahmad, M. u. N. Tariq, *et al.*,Life Cycle Assessment of Lithium-ion Batteries: A Critical Review, *Resour., Conserv. Recycl.*, 2022, 106164.
57 A. Thielmann, R. Isenmann and M. Wietschel, Technologie-Roadmap Vorwort, *Fraunhofer ISI*, 2010, 3–22.
58 F. Lorandi, T. Liu, M. Fantin, J. Manser, A. Al-Obeidi, M. Zimmerman, *et al.*,Comparative performance of ex situ artificial solid electrolyte interphases for Li metal batteries with liquid electrolytes, *iScience*, 2021, 102578.
59 R. Koerver, I. Aygün, T. Leichtweiß, C. Dietrich, W. Zhang, J. O. Binder, *et al.*,Capacity Fade in Solid-State Batteries: Interphase Formation and Chemomechanical Processes in Nickel-Rich Layered Oxide Cathodes and Lithium Thiophosphate Solid Electrolytes, *Chem. Mater.*, 2017, 5574–5582.
60 Y. Benabed, M. Rioux, S. Rousselot, G. Hautier and M. Dollé, Assessing the Electrochemical Stability Window of NASICON-Type Solid Electrolytes, *Front. Energy Res.*, 2021, 1–13.
61 T. Yoshinari, R. Koerver, P. Hofmann, Y. Uchimoto, W. G. Zeier and J. Janek, Interfacial Stability of Phosphate-NASICON Solid Electrolytes in Ni-Rich NCM Cathode-Based Solid-State Batteries, *ACS Appl. Mater. Interfaces*, 2019, 23244–23253.
62 M. Rosen, M. Finsterbusch, O. Guillon and D. Fattakhova-Rohlfing, Free standing dual phase cathode tapes-scalable fabrication and microstructure optimization of garnet-based ceramic cathodes, *J. Mater. Chem. A*, 2022, 2320–2326.
63 M. Ihrig, E. Dashjav, A. M. Laptev, R. Ye, D. Grüner, M. Ziegner, *et al.*,Increasing the performance of all-solid-state Li batteries by infiltration of Li-ion conducting polymer into LFP-LATP composite cathode, *J. Power Sources*, 2022, 231822.
64 K. J. Kim and J. L. M. Rupp, All ceramic cathode composite design and manufacturing towards low interfacial resistance for garnet-based solid-state lithium batteries, *Energy Environ. Sci.*, 2020, 4930–4945.
65 ISO (International Organization for Standardization), ISO 14040: Environmental management—Life cycle assessment—Principles and framework, *Environ. Manage.*, 2006, 28.
66 ISO (International Organization for Standardization), *Environmental management: life cycle assessment; requirements and guidelines*, ISO Geneva, 2006.
67 Sphera Solutions GmbH, *GaBi (Ganzheitliche Bilanzierung) version10.6. 2022 2022-03-01*, Available from: **https://gabi.sphera.com**.
68 *Ecoinvent, Life Cycle Inventory Database Version 3.7.1*, Swiss Center for Life Cycle Inventory, St. Gallen, Switzerland, 2020.
69 M. A. J. Huijbregts, Z. J. N. Steinmann, P. M. F. Elshout, G. Stam, F. Verones, M. Vieira, *et al.*,ReCiPe2016: a harmonised life cycle impact assessment method at midpoint and endpoint level, *Int. J. Life Cycle Assess.*, 2017, 138–147.
70 Y. Deng, J. Li, T. Li, X. Gao and C. Yuan, Life cycle assessment of lithium sulfur battery for electric vehicles, *J. Power Sources*, 2017, 284–295.
71 X. Sun, X. Luo, Z. Zhang, F. Meng and J. Yang, Life cycle assessment of lithium nickel cobalt manganese oxide (NCM) batteries for electric passenger vehicles, *J. Cleaner Prod.*, 2020, 123006.
72 M. O. Wittner, H. P. Karbstein and V. Gaukel, Spray drying of high viscous food concentrates: Investigations on the applicability of an Air-Core-Liquid-Ring (ACLR) nozzle for liquid atomization, *IDS'2018 – 21st International Drying Symposium*, 2019, 11–14.
73 G. A. Blengini, C. E. L. Latunussa, U. Eynard, C. Torres de Matos, D. Wittmer and K. Georgitzikis, *et al.,Study on the EU's list of Critical Raw Materials (2020) Final Report*, 2020.
74 O. Winjobi, J. C. Kelly and Q. Dai, Life-cycle analysis, by global region, of automotive lithium-ion nickel manganese cobalt batteries of varying nickel content, *Sustainable Mater. Technol.*, 2022, e00415.